High concentration of cobalt in the Ajabgarh rocks of Delhi Supergroup, Southwest Haryana, India

Naresh Kumar[1], Swati Rana[1,*] and A. Krishnakanta Singh[2]

[1]Department of Geology, Kurukshetra University, Kurukshetra 136 119, India
[2]Wadia Institute of Himalayan Geology, Dehradun 240 001, India

In this study, we report a high concentration of cobalt (Co) in the rocks of Ajabgarh Group of Delhi Supergroup from Nasibpur and the surrounding areas of Southwest Haryana, India, which forms a part of the North Delhi Fold Belt (NDFB). Metasedimentary and magmatic phases of the rocks contained high cobalt content ranging from 166 to 3657 ppm. The maximum concentration of cobalt (2371–3657 ppm) was observed in quartzite samples from the Nasibpur area. Cobalt enrichment in these rocks can be attributed to magmatic–hydrothermal and metamorphic fluids in relation to geological features such as shear and foliation zones, which provide a high fluid/rock ratio. Overall, the applications of cobalt are numerous and crucial. The present study warrants further extensive exploration efforts in order to assess the abundance of this valuable metal, as the global cobalt market is increasing in response to a low-carbon economy.

Keywords: Cobalt, low carbon economy, metamorphic fluids, quartzite, sedimentary rocks.

COBALT (Co) can be found in diverse geological settings such as intracratonic structurally controlled replacement deposits, which may be hydrothermal or magmatic in origin (also known as iron oxide–Cu–Au–Ag–U–REE–Co–Ni)[1,2], metasediment-hosted Co–Cu–Au, stratiform sediment-hosted Cu–Co (SSHC)[3], black shale-hosted[4], Ni–Co laterite[5,6], polymetallic Co-rich veins[7–9], and skarn and replacement deposits[10]. Among these, SSHC magmatic Ni–Cu–Co (platinum group element (PGE)) and Ni–Co laterite deposits host 85% of the global cobalt resources. In sedimentary rocks, siliciclastic and carbonates such as dolomitic limestone and dolomite-rich shale host cobalt deposits in Zambia and the Democratic Republic of Congo (DRC) in Central Africa, which has the world's highest concentration of copper and cobalt[11,12]. Globally, these are located in the Bou–Azzer deposit (Morocco), Idaho cobalt belt, Blackbird district (USA), Cobalt Gowganda (Canada) and Olympic Dam (Australia). Table 1 presents the cobalt concentration in some of the major deposits across the world. In the present study, many samples contain cobalt concentrations higher than the minimum grade (300 ppm) or cut-off grade (200 ppm) for sulphide or arsenide commercial exploitation. Due to its unique properties like high melting point (1495°C), highest known Curie point (1121°C) and several oxidation states, cobalt has a broad range of applications as superalloys, magnetic alloys, high-speed steels, etc.

The 'Delhi system' represents rocks from northeast Rajasthan to Gujarat deposited in spatially separated basins to form a single synchronous lithostratigraphic region[13,14]. On the basis of two distinct intrusive magmatic events, the Delhi basin further evolved into the North Delhi Fold Belt (NDFB; NE Rajasthan with multidepocentres) and the younger South Delhi Fold Belt (western and central area of the Aravalli Mountain Range)[15,16]. The NDFB comprises three distinct sediment repositories: Khetri, Alwar and Lalsot–Bayana sub-basins[17]. The Delhi supergroup rocks have been subdivided stratigraphically into three groups, viz. Raialo (dominantly carbonate–arenite), Alwar (dominantly arenite) and Ajabgarh (dominantly metabasic and pelitic calcareous)[14]. The present study was carried out at Nasibpur hills and surrounding areas such as Raghunathpura and Kirarod ki dhani (28°4′50″N and 76°6′22″E) in Mahendragarh district, Southwest Haryana, India (Figure 1), where the metasedimentary (garnet mica schist, amphibolite, marble, quartzite, phyllites and granitic gneiss) and magmatic (granite, pegmatite and quartz veins) phases of rocks are exposed in the isolated and linear ridges which form a part of NDFB. This Belt is intruded by various granitoid plutons in the range 1850–1700 Ma (refs 18–20). These activities are considered the source providing the necessary hydrothermal fluids to reactivate the mineralized system. The mineralization in NDFB has been recorded in different lithological units like scapolite, tremolite-rich calc-silicate rocks, amphibole-rich marble and quartz–carbonate veins, which is also structurally controlled within foliation planes and shear zones[21,22]. The average cobalt concentration in the upper continental crust was 10 ppm, and in the bulk continental crust, it was 35 ppm (ref. 23). All samples from the study area had higher cobalt concentration in comparison to the above-mentioned average concentration of cobalt in the upper and bulk continental crust (except samples KD-4I and RP-13).

The occurrence of high cobalt was noted in samples of the zone with folding and fracturing of rocks sandwiched due to high pressure. This was evident by the presence of garnet mica schist as an increasing grade of metamorphism in the area (Figure 2 *a*). The associated sulphide mineralization was observed in host rock quartzite (Figure 2 *b*). The radial pattern of amphibole minerals was visible with sulphide mineralization (Figure 2 *c*). A highly mineralized surface on brown quartzite was also observed (Figure 2 *d*). The role of meteoric and magmatic fluids has been emphasized by researchers in different cobalt deposits globally, particularly in DRC[24] and the Bou Azzer deposit in Morroco[25], in response to an increase in pH. Various alteration patterns like albitization, chlorite, muscovite and biotite alteration associated with Co enrichment have been studied in the rocks[26,27]. The carbonates in the study area also

*For correspondence. (e-mail: swatirana4567@gmail.com)

Table 1. Cobalt (Co) concentration in some of the major deposits of the world and in rocks (world average)

Deposit	Co %	Co (ppm)	Rock type	Co (ppm)	Reference
Black bird deposits, USA	0.58	5,800	Ultramafic	200	42
Fredericktown, USA	0.27	2,700	Dunite	108.6	43
Mount cobalt, Australia	0.05	500	Pyroxenite	55.2	43
Joumasuo, Finland	0.2	2,000	Serpentinite	115.1	43
Haarkumpu, Finland	0.17	1,700	Mafic	45.0	42
Outokumpu, Finland	0.13	1,300	Gabbro	51.0	44
Sotkamo, Finland	0.29	2,900	Basalt	41.0	44
Werner Lake, Canada	1.68	16,800	Granite	47.0	42
Modum, Norway	0.26	2,600	Felsic	5.0	42
Olympic Dam, Australia	0.04	400	Shales	19	42
Magnitogorsk, Russia	0.02	200	Carbonates	0.1	42
Bou-Azzer, Morocco	0.02	200	Sandstone	0.3	42
Cobalt Gowganda, Canada	0.02	200	Schist	40	25
Mutanda, Democratic Republic of Congo	0.29	2,900	Quartzite	0.3	25

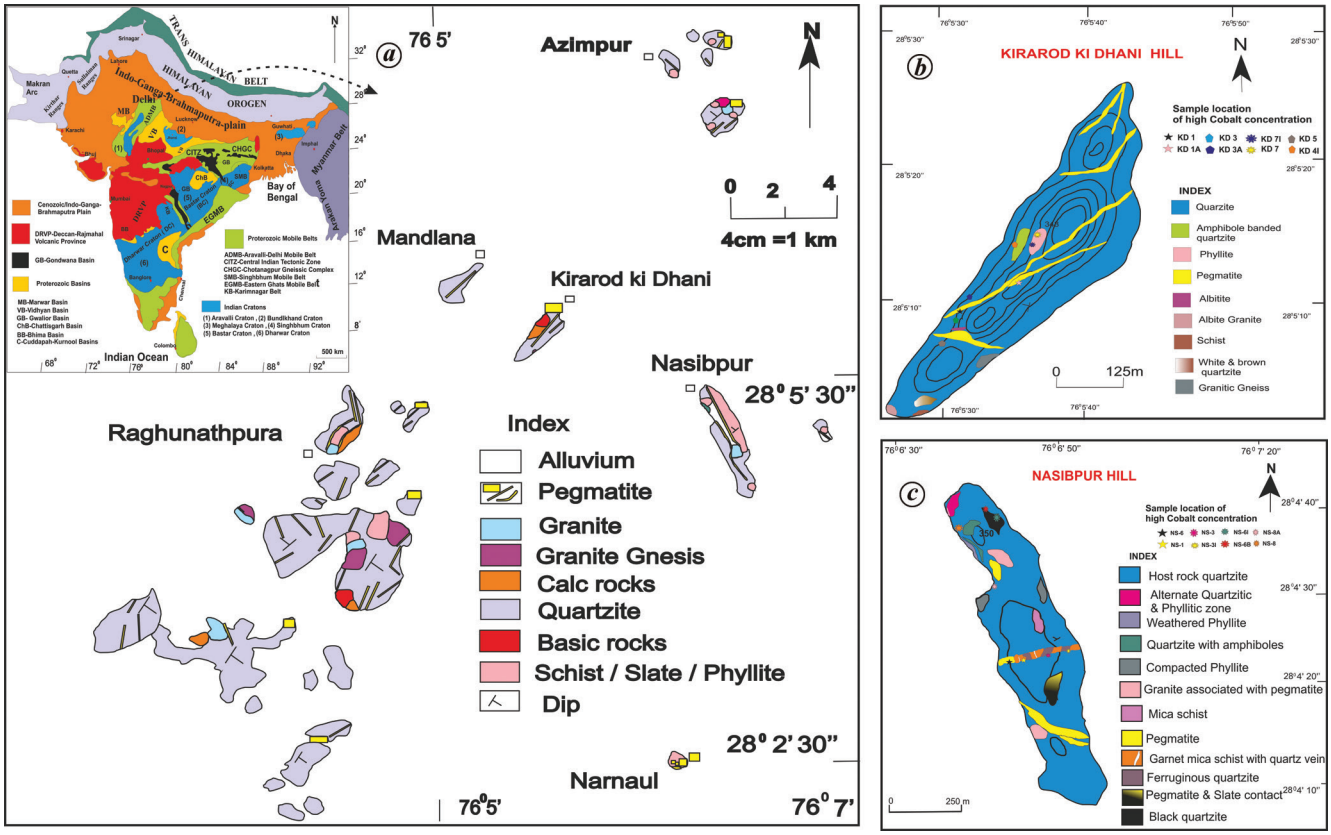

Figure 1. ***a***, Geological map of Nasibpur and surrounding areas, Haryana, India. (Inset) Map showing the location of Aravalli orogen. ***b***, ***c***, Detailed geological map of (***b***) Kirarod ki dhani hill and (***c***) Nasibpur hill showing cobalt (Co) enrichment zones.

indicate CO_2 mobilization due to metamorphic recrystallization, which reflects the significance of organic materials in the reduction of Co enrichment[28]. The pyrite veins in which sulphide is interstitial with silicates in the alteration zones have been identified with cobalt enrichment (Figure 3 *a*). In Figure 3 *e*, biotite alteration along with albite can be seen associated with fractures in the rocks where high Co concentration occurs. The morphological, distribution and geochemical studies on sulphides have shown that in pentlandite cobalt is usually isomorphically substituted for Ni^{2+} (ref. 29). The euhedral Co-bearing pyrite shows zonation in the pelitic mineral rock matrix (Figure 3 *b*). Cobalt-bearing minerals are associated with alteration pattern like scapolitization in the area, which can be seen along with the foliation plane (Figure 3 *c*). Understanding the mineralization processes of nickel and cobalt requires the identification of several mineralization stages. In the study area, Co-bearing sulphides have been identified in relict texture

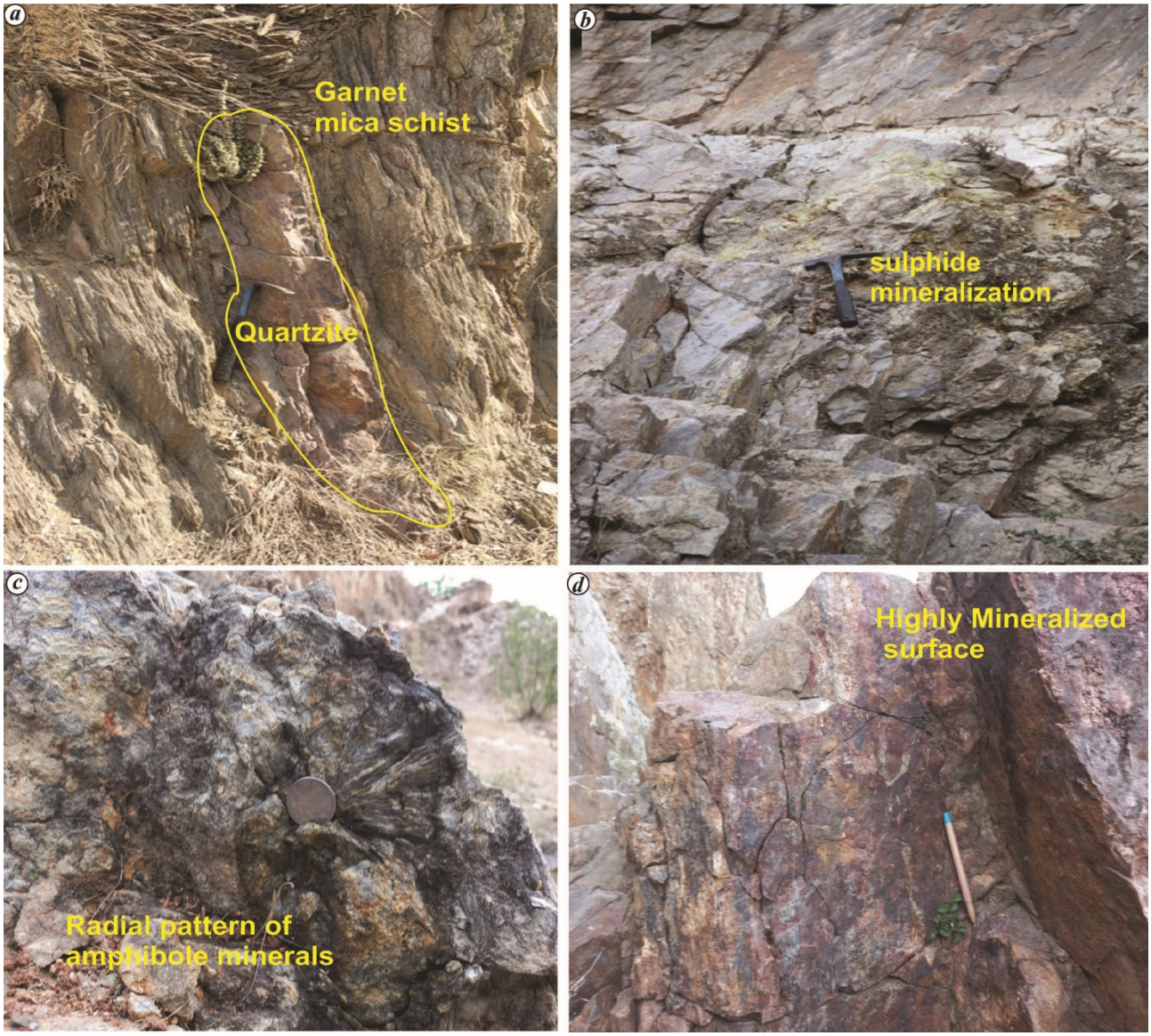

Figure 2. ***a***, Contact between garnet mica schist and brown quartzite showing increasing grade of metamorphism. ***b***, Sulphide mineralization in host rock quartzite. ***c***, Radial pattern of amphibole minerals with sulphide mineralization. ***d***, Highly mineralized surface in brown quartzite.

(Figure 3 *d*), with the pentlandite grains intergrown at the rims of Co-bearing phases in the microcracks (Figure 3 *f*). An alteration pattern is visible where albite and biotite are present in rocks with high Co concentration with quartz and tourmaline (Figure 3 *e*). The textural relationship of cobalt-rich minerals and sulphides can be seen as the cobalt mineral phases are enclosed within sulphides and show replacement with pentlandite grains at the rims as evidenced by the fine-grained, porous and finely fractured characteristics, either as a result of hydrothermal alteration or weathering[30,31]. Possibly, the cobalt enrichment in the study area is linked to metamorphic terranes where different fluid types, such as magmatic–hydrothermal and metamorphic, lead to their concentration in the rocks. Also, cobalt enrichment in the faults and fractures produces cobalt-rich vein deposits in metasedimentary and metaigneous rocks of the Proterozoic age[32]. The prominent presence of Co in sulphides implies a relatively reducing environment. The physical and chemical conditions of the fluid system have a significant impact on the cobalt concentration in sulphides/sulphoarsenides[33,34].

Furthermore, cobalt is also concentrated in metamorphosed siliciclastic strata mainly of Proterozoic age with varied origin, which consists of a range of mineralizing processes including cobaltiferous pyrite, biotite, quartz, albite, scapolite and muscovite taking place before and after metamorphism. Studies have also linked these types of deposits with granitic plutons[3,10]. The presence of various alteration products like scapolitization, sulphidization and albitization in the study area demonstrates the role of fluids and a key process for cobalt precipitation. The precipitation of cobalt can

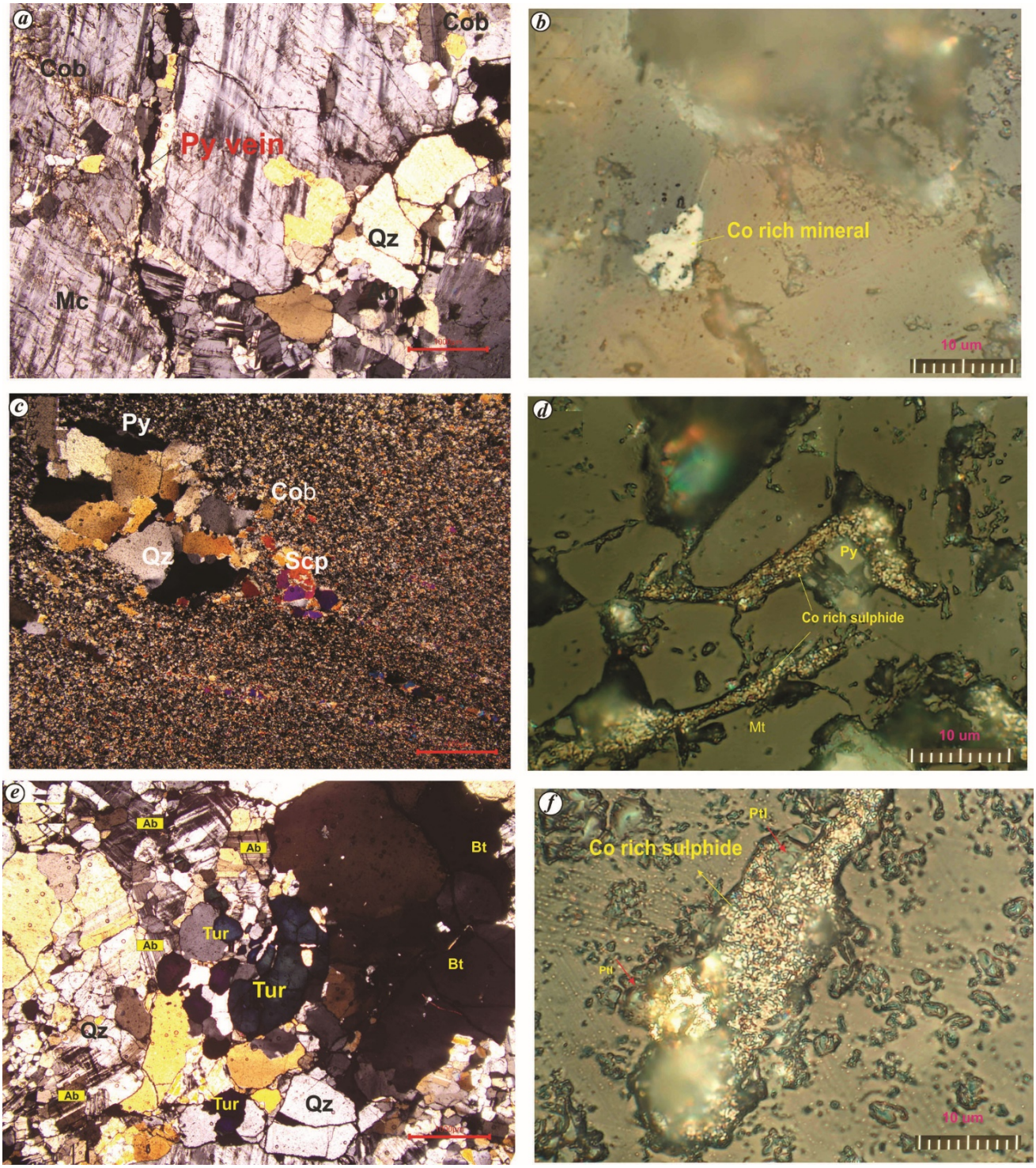

Figure 3. ***a***, Pyrite vein associated with microcline and quartz grains. ***b***, Euhedral Co-bearing pyrite. ***c***, Scapolitization with pyrite grains along the foliation plane. ***d***, Co-bearing phases enclosed in sulphide. ***e***, Albite grains showing replacement texture with quartz, biotite and tourmaline. ***f***, Cobalt-rich sulphide/sulphoarsenide with pentaldite rims.

be seen along veins, fissures and cracks as metasomatic replacements aided by hydrothermal fluids. Analysis of cobalt concentration was done at the Wadia Institute of Himalayan Geology, Dehradun, using X-ray fluorescence (XRF; Bruker Tiger S-8) on pressed-powder pellets, with a precision of ±5–6%. Table 2 shows the cobalt concentration in the examined rocks of the study area.

This enrichment of cobalt is revealed by pegmatites (167–519 ppm), phyllite (557–615 ppm), garnet mica schist (166 ppm) and quartzite (30–3657 ppm) in the study

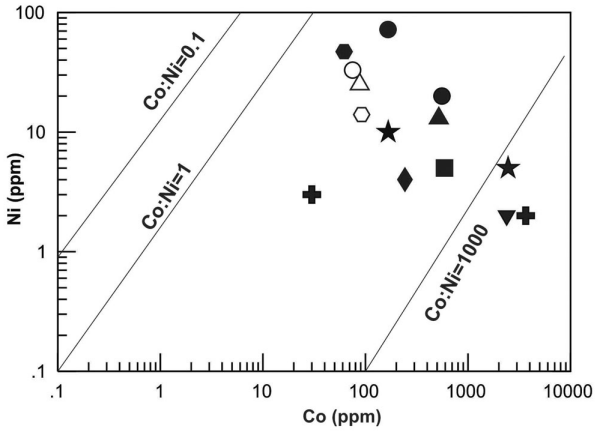

Figure 4. Samples from the study area falling in the zone of hydrothermal origin where Co : Ni ratio is greater than 1.

Table 2. Cobalt concentration in the rocks of Ajabgarh group, Delhi Supergroup from Nasibpur and surrounding areas, Southwest Haryana, India

Sample	Location	Rock type	Cobalt concentration (ppm)
NS-8	Nasibpur	Quartzite	3,657
NS-8A	Nasibpur	Quartzite	3,587
NS-6B	Nasibpur	Quartzite	2,488
NS-6I	Nasibpur	Quartzite	2,463
NS-3	Nasibpur	Quartzite	2,387
NS-3I	Nasibpur	Quartzite	2,371
KD-3	Kirarod ki Dhani	Quartzite	607
KD-3A	Kirarod ki Dhani	Quartzite	591
KD-5	Kirarod ki Dhani	Quartzite	243
KD-7I	Kirarod ki Dhani	Phyllite	615
KD-7	Kirarod ki Dhani	Phyllite	557
KD-1	Kirarod ki Dhani	Pegmatite	519
KD-1A	Kirarod ki Dhani	Pegmatite	487
NS-6	Nasibpur	Pegmatite	167
NS-1	Nasibpur	Garnet mica schist	166
RP-1A	Raghunathpura	Quartzite	92
RP-1	Raghunathpura	Quartzite	88
RP-7	Raghunathpura	Granite Gneiss	62
RP-13	Raghunathpura	Amphibole Quartzite	30
KD-4I	Kirarod ki Dhani	Amphibole Quartzite	30

Table 3. Geochemical results of the studied samples having high Co concentration

Sample	SiO_2 (%)	Fe_2O_3 (%)	Na_2O (%)	K_2O (%)	Al_2O_3 (%)	Cu (ppm)	Pb (ppm)	Ni (ppm)
KD-1	73.89	0.43	5.86	5.00	15.16	4	92	13
KD-3	85.88	0.98	0.64	0.29	1.79	12	6	5
KD-5	79.14	1.00	0.70	0.14	1.14	10	5	4
KD-7	87.27	0.79	0.78	2.32	6.38	38	75	20
NS-3	94.33	2.46	0.16	0.41	2.30	39	6	2
NS-6	63.79	1.17	5.24	3.65	22.18	8	59	10
NS-6I	>95.9	0.67	0.17	0.38	0.87	25	93	5
NS-8	>95.9	0.73	0.20	0.31	0.87	15	10	2
KD-4I	50.98	5.01	0.99	0.29	2.39	4	11	3
NS-1	53.73	7.27	0.66	5.66	23.04	43	6	72
RP-7	55.11	5.65	1.38	4.50	11.52	BDL	15	47
RP-13	52.38	3.29	0.84	0.36	2.19	2	BDL	BDL
NS-5	58.47	15.75	0.11	3.07	8.62	25	7	33
RP-1	70.42	1.65	1.86	2.92	7.75	54	30	25
RP-1A	73.21	2.15	0.97	0.38	2.74	18	8	14

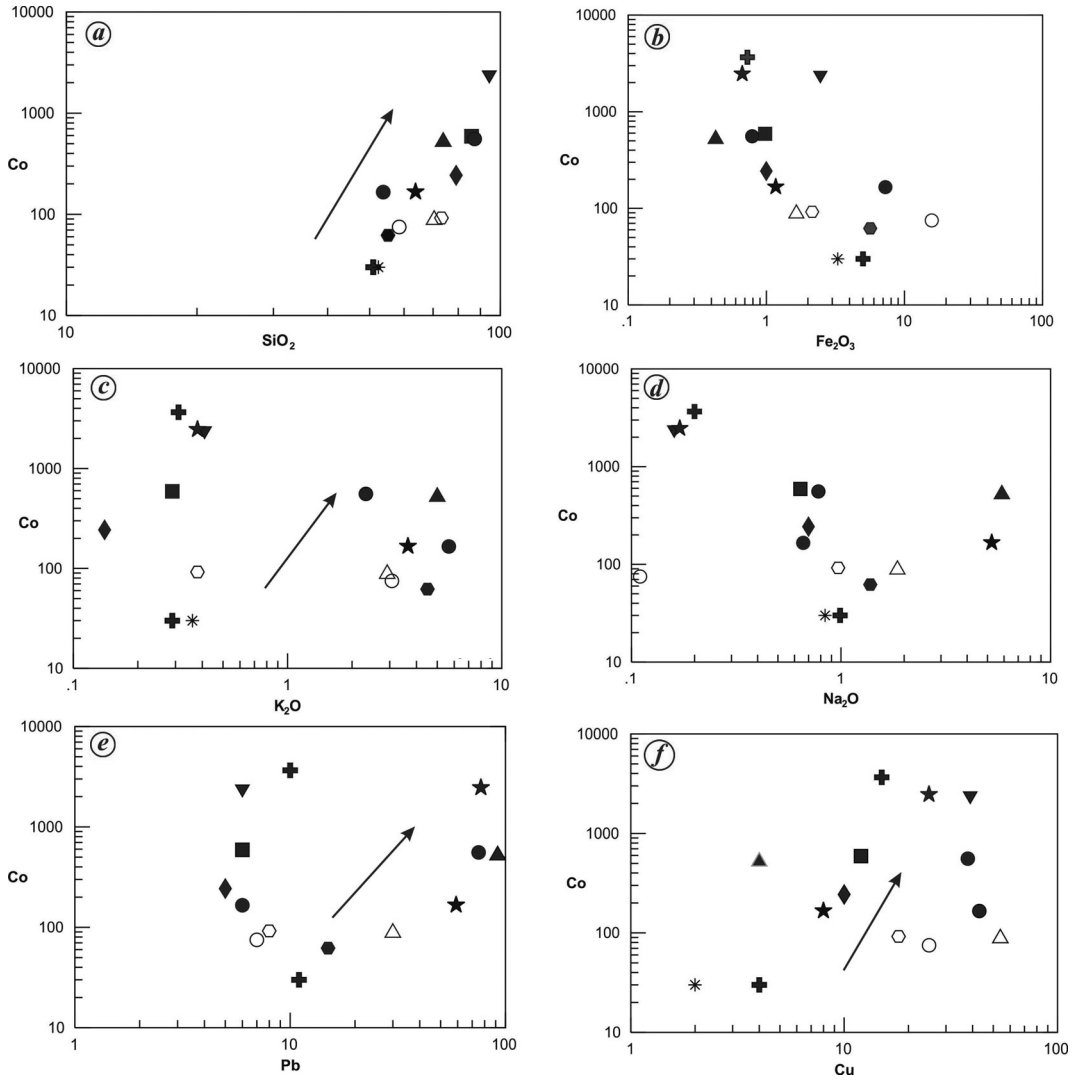

Figure 5. Binary diagrams of selected elements from whole-rock analyses of samples. ***a***, Co versus SiO_2; ***b***, Co versus Fe_2O_3; ***c***, Co versus Na_2O; ***d***, Co versus K_2O; ***e***, Co versus Pb; ***f***, Co versus Cu.

area. Quartzites are classified into two groups on the basis of cobalt enrichment, where one group showed a 30–92 ppm concentration of cobalt, while the other had the highest concentration in the range of 243–3657 ppm. Maximum enrichment was shown by quartzites of Nasibpur Hill, viz. NS-3 (2387 ppm), NS-3I (2371 ppm), NS-6B (2488 ppm), NS-6I (2463 ppm), NS-8A (3587 ppm), NS-8 (3657 ppm), which is very high in comparison with the world's average cobalt concentration in quartzite (0.3 ppm)[30]. This enrichment can be correlated with the presence of brecciation, fracturing and foliation planes, which create a network for a high fluid/rock ratio. The amphibole-bearing quartzites (KD-4I and RP-13) showed a cobalt concentration of 30 ppm, whereas the compacted grey–brown-coloured quartzite samples (NS-6I, NS-6B, NS-8, NS-8A) showed very high values ranging from 2463 to 3657 ppm. The hydrothermal alteration pattern was visible in the study area, indicating the role of fluids that aid the replacement processes with associated sulphide mineralization. Phyllite sample contained 557–615 ppm cobalt concentration, and schist contained 167 ppm cobalt, which is also high relative to the world average concentration (40 ppm)[35]. The Co: Ni ratio in the samples was greater than 1, indicating its magmatic-hydrothermal origin (Figure 4).

The nature of the rocks and their mineralogical aspects must be considered when determining the possible mobility of trace elements. Table 3 shows the results of the geochemical analysis of the samples with a high cobalt concentration. The siliceous rocks contained high Co concentration and showed a positive correlation. The quartzites, phyllites and pegmatites contained high SiO_2, ranging from 73.21% to 95.9%. Correlation analysis also showed a weak to moderate positive correlation with Fe_2O_3, Pb and Cu, while some samples also showed a strong correlation with Na_2O and K_2O (Figure 5). The pegmatite samples with Co enrichment also showed high Na_2O (5.24–5.84%) and high Al_2O_3 (15.16–22.18%). Co-bearing sulphide mineral phases were also revealed by sulphide saturation in the magma

during a significant amount of crustal material contamination[36]. Due to the high partition coefficient between sulphide and silicate melts, nickel and cobaltite tend to enrich the sulphide melt when sulphide saturation occurs in the magma[37].

The pH and temperature of weathering solutions play a major role in the amount of cobalt dissolved and transported. This is because cobalt is often predominantly transported in sulphide and arsenide minerals in octahedral and tetrahedral sites due to increased entropy with temperature in hydrothermal solutions[38]. As the study area comprises various mineral assemblages like amphiboles, phyllosilicates, carbonates and garnet, it indicates the varied range of temperature and pressure conditions in the area, which is important for cobalt enrichment and has the potential to increase its mobility to form various cobalt complexes. In addition, it is likely to be mobile under some weathering conditions due to the instability of cobalt complexes with temperature and the dilution of saline fluid near the Earth's surface that results in its precipitation[39]. Co-precipitation has been explained by an increase in oxygen and sulphur fugacity along with a drop in temperature as an important factor in the magmatic–hydrothermal fluid system[40]. The study on cobalt mineralization infers that hydrothermal systems incorporating oxidized brines have a stronger potential to transport and leach significant rock volumes of Co and Ni at any temperature or realistic pH (ref. 28). Therefore, various geological processes like magmatic processes (differentiation and fractional crystallization), hydrothermal activity and chemical weathering play a crucial role in Co concentration in the rocks of the study area. The results of the present study call for further research to assess the cobalt resource in the study area. The global cobalt market is showing an increasing trend due to its wide variety of applications. So there is a need to understand its mineralization parameters in line with Government targets to achieve global climate goals as reaffirmed by the Paris Agreement in 2015 (ref. 41). The following conclusions can be drawn from the present study: (i) Several rocks contain high Co concentration in the study area, especially quartzites (2371–3657 ppm). (ii) Co is primarily found in pyrite and Co-rich sulphides/sulphoarsenides, making it a potential Co resource, as the minimum cut-off grade for Co in sulphides is 300 ppm.

1. Williams, S. R. and Richardson, J. M., Geometallurgical mapping: a new approach that reduces technical risks. In Proceedings of 36th Annual Meeting of the Canadian Mineral Processors Conference, CIM, Ottawa, Canada, 2004, pp. 241–268.
2. BHP Group Ltd, Annual Report 2019; https://www.bhp.com/investor-centre/-/media/documents/investors/annual-reports/2019/bhpannualreport2019.pdf
3. Slack, J. F. (ed.), Descriptive and geoenvironmental model for cobalt–copper–gold deposits in metasedimentary rocks. Scientific Investigations Report 2010-5070-G, US Geological Survey, Reston, Virginia, 2019.
4. Gregory, D. D., Large, R. R. and Halpin, J. A., Trace element content of sedimentary pyrite in black shale. *Econ. Geol*., 2015, **110**(6), 1389–1410.
5. Berger, V. I., Mosier, D. L., Bliss, J. D. and Moring, B. C., Sediment-hosted gold deposits of the world: database and grade and tonnage models. Open-File Report, 2014, 1074, p. 51.
6. Decr´ee, S., Pourret, O. and Baele, J. M., Rare earth element fractionation in heterogenite (CoOOH): implication for cobalt oxidized ore in the Katanga Copperbelt (Democratic Republic of Congo). *J. Geochem. Explor*., 2015, **159**, 290–301.
7. Nimis, P., Costa, D. L. and Guastoni, A., Cobaltite-rich mineralization in the iron skarn deposit of Traversella (Western Alps, Italy). *Mineral. Mag*., 2014, **78**, 11–27.
8. Naumov, G. B., Golubev, V. N., Vlasov, B. P. and Mironov, O. F., The Schlema–Alberoda five-element uranium deposit, Germany: an example of self-organizing hydrothermal system. *Geol. Ore. Deposit*, 2017, **59**, 1–13.
9. Zou, S., Zou, F., Ning, J., Deng, T., Yu, D., Xu, D. and Wang, Z., A stand-alone Co mineral deposit in northeastern Hunan Province, South China: its timing, origin of ore fluids and metal Co, and geodynamic setting. *Ore Geol. Rev*., 2018, **92**, 42–60.
10. Slack, J. F., Kimball, B. E. and Shedd, K. B., Cobalt. In *Critical Mineral Resources of the United States – Economic and Environmental Geology and Prospects for Future Supply* (eds Schulz, K. *et al.*), US Geological Survey Professional Paper 1802, Reston, Virginia, USA, 2017, pp. F1–F40.
11. Kampunzu, A. B., Tembo, F., Matheis, G., Kapenda, D. and Huntsman-Mapila, P., Geochemistry and tectonic setting of mafic igneous units in the Neoproterozoic Katangan Basin, Central Africa: implications for Rodinia break-up. *Gondwana Res.*, 2000, **3**, 125–153.
12. Cailteux, J. L. H., Kampunzu, A. B., Lerouge, C., Kaputo, A. K. and Milesi, J. P., Genesis of sediment-hosted stratiform copper–cobalt deposits, central African Copperbelt. *J. Afr. Earth Sci*., 2005, **42**, 134–158.
13. Heron, A. M., Geology of north-eastern Rajputana and adjacent districts. *Mem. Geol. Surv. India*, 1917, **45**, 128.
14. Heron, A. M., The Geology of central Rajputana. *Mem. Geol. Surv. India*, 1953, **79**, 389.
15. Choudhary, A., Gopalan, K. and Sastry, C. A., Present status of the geochronology of the Precambrian rocks of Rajasthan. *Tectonophysics*, 1984, **105**, 131–140.
16. Sinha Roy, S., Proterozoic Wilson Cycles in Rajasthan, NW India. *Mem. Geol. Soc. India*, 1988, **7**, 95–107.
17. Roy, A. B. and Jakhar, S. R., *Geology of Rajasthan: Precambrian to Recent*, Scientific Publisher, Jodhpur, 2002, p. 421.
18. Biju-Sekhar, S., Yokoyama, K., Pandit, M. K., Okudaira, T., Yoshida, M. and Santosh, M., Late Paleoproterozoic magmatism in Delhi Fold Belt, NW India and its implication: evidence from EPMA chemical ages of zircons. *J. Asian Earth Sci*., 2003, **22**, 89–207.
19. Kaur, P., Chaudhri, N., Raczek, I., Kroner, A. and Hofman, A., Geochemistry, zircon ages and whole-rock Nd isotopic systematics for Palaeoproterozoic A-type granitoids in the northern part of the Delhi belt, Rajasthan, NW India: implications for late Palaeoproterozoic crustal evolution of the Aravalli craton. *Geol. Mag*., 2007, **144**, 361–378.
20. Kaur, P., Zeh, A., Chaudhri, N. and Eliyas, N., Two distinct sources of 1.73–1.70 Ga A-type granites from the northern Aravalli orogen, NW India: constraints from *in-situ* zircon U–Pb ages and Lu–Hf isotopes. *Gondwana Res*., 2017, **49**, 164–181.
21. Singh, Y., Pandit, P. S. C., Bagora, S. and Jain, P. K., Mineralogy, geochemistry, and genesis of co-genetic granite pegmatite-hosted rare metal and rare earth deposits of the Kawadgaon area, Bastar Craton, Central India. *J. Geol. Soc. India*, 2012, **89**, 115–130.
22. Baidya, A. S., Sen, A. and Pal, D. C., Textures, and compositions of cobalt pentlandite and cobaltian mackinawite from the Madan–Kudan copper deposit, Khetri Copper Belt, Rajasthan, India. *J. Earth Syst. Sci*., 2018, **127**, 58.
23. Taylor, S. R. and McLennan, S. M., *The Continental Crust: Its Composition and Evolution*, Blackwell, Oxford, UK, 1985, pp. 1–312.

24. Roberts, S. and Gunn, G., Cobalt. In *Critical Metals Handbook* (ed. Gunn, G.), British Geological Survey, John Wiley, UK, 2014, pp. 122–149.
25. Carr, M. H. and Turekian, K. K., The geochemistry of cobalt. *Geochim. Cosmochim. Acta*, 1961, **23**, 9–60.
26. Vanhanen, E., Geology, mineralogy, and geochemistry of the Fe–Co–Au–(U) deposits in the Paleoproterozoic Kuusamo Schist Belt, northeastern Finland. *Geol. Surv. Finland Bull.*, 2001, **399**, 398.
27. Witt, W. K., Davies, A. and Hagemann, S. G., Multi-stage alteration and multiple fluid inputs for the Paleoproterozoic Juomasuo, Hangaslampi and Haarakumpu cobalt (-Au-REE) deposits of the Kuusamo Schist Belt, Finland. In IAGOD Conference, Salta, Argentina, Abstr., 2018.
28. Jansson, N. F. and Weihua, L., Controls on cobalt and nickel distribution in hydrothermal sulphide deposits in Bergslagen, Sweden – constraints from solubility modelling. *GFF*, 2020, **142**(2), 87–95.
29. Feng, C. Y., Zhao, Y. M., Li, D. X., Liu, J. N. and Liu, C. Z., Mineralogical characteristics of the Xiarihamu nickel deposit in the Qiman Tagh mountain, East Kunlun, China. *Geol. Rev*., 2016, **62**, 215–228.
30. Tenailleau, C., Pring, A., Etschmann, B., Brugger, J., Grguric, B. and Putnis, A., Transformation of pentlandite to violarite under mild hydrothermal conditions. *Am. Mineral*, 2006, **91**, 706–709.
31. Xia, F., Brugger, J., Chen, G., Ngothai, Y., O'Neill, B. and Putnis, A., Mechanism and kinetics of pseudomorphic mineral replacement reactions: a case study of the replacement of pentlandite by violarite. *Geochem. Cosmochim. Acta*, 2009, **73**, 1945–1969.
32. Kissin, S. A., Five-element (Ni–Co–As–Ag–Bi) veins. *Geosci. Can*., 1992, **19**(3), 113–124.
33. Velásquez, G., Béziat, D., Salvi, S., Siebenaller, L., Borisova, A. Y., Pokrovski, G. S. and De Parseval, P., Formation and deformation of pyrite and implications for gold mineralization in the El Callao District, Venezuela. *Econ. Geol*., 2014, **109**, 457–486.
34. George, L. L., Cook, N. J. and Ciobanu, C. L., Partitioning of trace elements in co-crystallized sphalerite–galena–chalcopyrite hydrothermal ores. *Ore Geol. Rev*., 2016, **77**, 97–116.
35. Ahmed, A. H., Arai, S. and Ikenne, M., Mineralogy and paragenesis of the Co–Ni arsenide ores of bou Azzer, Anti-Atlas, Morocco. *Econ. Geol*., 2009, **104**, 249–266.
36. Liu, Y., Li, W., Jia, Q., Zhang, Z., Wang, Z. and Zhang, Z., The dynamic sulfide saturation process and a possible slab break-off model for the giant Xiarihamu magmatic nickel ore deposit in the East Kunlun orogenic belt, northern Qinghai–Tibet plateau, China. *Econ. Geol*., 2018, **113**, 1383–1417.
37. Li, Y. and Audétat, A., Partitioning of V, Mn, Co, Ni, Cu, Zn, As, Mo, Ag, Sn, Sb, W, Au, Pb, and Bi between sulfide phases and hydrous basanite melt at upper mantle conditions. *Earth Planet Sci. Lett*., 2012, **355**, 327–340.
38. Muchez, Ph. and Corbella, M., Factors controlling the precipitation of copper and cobalt minerals in sediment-hosted ore deposits: advances and restrictions. *J. Geochem. Explor*., 2012, **118**, 38–46.
39. Liu, W., Borg, S. J., Testemale, D., Etschmann, B., Hazemann, J.-L. and Brugger, J., Speciation and thermodynamic properties for cobalt chloride complexes in hydrothermal fluids at 35–440°C and 600 bar: an *in-situ* XAS study. *Geochim. Cosmochim. Acta*, 2011, **75**, 1227–1248.
40. Wang, Z. *et al.*, Micro-textural and chemical fingerprints of hydrothermal cobalt enrichment in the Jingchong Co–Cu polymetallic deposit, South China. *Ore Geol. Rev*., 2022, **142**, 104721.
41. Cobalt Market Review 2019–2020, Darton Commodities Ltd, Guildford, UK, 2020.
42. Krauskopf, K. B. and Bird, D. K., *Introduction to Geochemistry*, McGraw Hill, New York, 1995, 3rd edn, p. 227.
43. Gülaçar, O. F. and Delaloye, M., Geochemistry of nickel, cobalt and copper in alpine-type ultramafic rocks. *Chem. Geol.*, 1976, **17**, 269–280.
44. Donaldson, J. D. and Bereysmann, D., Cobalt and cobalt compounds. In *Ullmann's Encyclopedia of Industrial Chemistry*, Wiley-VCH Verlag GmbH, KGaA, Weinheim, Germany, 2005.

ACKNOWLEDGEMENTS. We thank Kurukshetra University for providing funds under seed money grant for the year 2022–23 (No. DPA-I/32/22/MRP/2358-2500). We also thank the Director, Wadia Institute of Himalayan Geology, Dehradun, for providing the analytical facilities.

Received 19 December 2022; revised accepted 12 June 2023

doi: 10.18520/cs/v125/i4/428-435

Neoarchaean stromatolites from the Dharwar Supergroup, India

Chethan Kumar[1], Yogmaya Shukla[2,*], Mukund Sharma[2], S. B. Harish Kumar[3], N. Malarkodi[1] and Saleem Ahmed Khan[4]

[1]Department of Geology, Bangalore University, Bengaluru 560 056, India
[2]Birbal Sahni Institute of Palaeosciences, 53 University Road, Lucknow 226 007, India
[3]Bhoogarbhdhama, No. 19, 1st Main, 4th Cross Road, New Maruthi Nagar Extension, Near MEI International School, Kempapura Road, Chikkabanavara, Bengaluru 560 090, India
[4]No. 291, JHBCS Layout, Near Dayanand Sagar College, Bengaluru 560 111, India

A new occurrence of Neoarchean stromatolite, older than 2600 Ma, has been found in the dolomite beds of Aleshpur Formation of the Chitradurga Group in the Shimoga Schist Belt, western Dharwar Craton. The occurrence is near Shanti Sagara lake (Sulekere) in the Davangere district of Karnataka. Stratiform, laminated, columnar with some showing branching forms indicate an advanced stage of evolution of stromatolites. The newly found stromatolite occurrence is an important addition to the inventory of Archaean stromatolites.

Keywords: Archaean, Dharwar Craton, Shimoga Schist Belt, stromatolite.

GLOBALLY, Neoarchaean carbonate rocks with palaeobiological signatures such as stromatolites are rare. Any report of such an occurrence of Archaean stromatolites from a new geographical locality or stratigraphic level is therefore important to the global inventory[1–4]. In 2008, two of us (S.B.H.K. and S.A.K.), while prospecting for minerals in the Archaean Dharwar Schist Belts, noted an outcrop of

*For correspondence. (e-mail: yogmayashukla@bsip.res.in)